TOWARDS THE DEVELOPMENT OF A FULL-SCALE TRANSIENT CFD MODEL TO SIMULATE THE STATIC AND DYNAMIC IN-CORE MASS FLUX DISTRIBUTION IN A CLASSICAL GERMAN PWR

Dong-Yuan Sheng
Westinghouse Electric Sweden AB
72163, Västerås, Sweden
shengd@westinghouse.com

Marcus Seidl
E.ON Kernkraft GmbH
Tresckowstrasse 5, 30457 Hannover, Germany
marcus.seidl@eon.com

ABSTRACT

In order to optimize the mechanical fuel design in a PWR not only the steady state flow field inside the core region is relevant but also the dynamic mass flux imbalances at the core inlet need to be known. Through induced cross flows these imbalances drive on the one hand potential grid-to-grid fretting damages and short-term variations in moderator-to-fuel ratio and on much longer time scales fuel assembly bow. From early scaled-down experiments it has been known for example, that the static mass flux profile across the core inlet varies in the order of about ±10% in a classical German 1300MWe PWR. Therefore it is of interest to understand how stable this mass flow pattern is as a function of time and how sensitive it is to small changes in thermal-hydraulic boundary conditions, e.g. a change in pump head or a change in downcomer eccentricity.

In order to start developing answers for these questions, a three-dimensional computational fluid dynamic (CFD) model including geometrical details in the lower plenum has been developed. A porous media model was used in the fuel-core region in the first stage of this work. Prior to CFD mesh generation a 3D CAD solid model has been built up. CFD results for pressure drop, flow distribution and mixing in downcomer and lower plenum have been analyzed to verify the model. The calculation results show a good agreement with experimental data. Future plan is to utilize the developed CFD model for thermal hydraulic analysis, such as lower plenum flow anomalies, boron dilution, thermal mixing and core flow distribution. The challenges for developing a large scale PWR vessel CFD model are discussed including large computing resource, numerical stability, and massive data management.

KEYWORDS
PWR, vessel CFD, pressure drop, flow distribution, mixing

1. INTRODUCTION

The knowledge of the flow distribution at the core inlet and along the active core zone in a classical German pressurized water reactor (PWR) is an important issue for a variety of safety analyses concerning the necessary hold-down forces of fuel assemblies, the maximum lateral forces on the fuel assemblies and for DNBR margin calculations in case of anticipated operating transients. Core inlet mass flux is influenced by the flow distribution between the loops and the mixing process in the downcomer and the lower plenum. This is a dynamic process driven by the turbulent flow itself and by small variations of

operating conditions. Usually the mass flux variations at the core inlet on average balance out over the first half of the active core region. Recently interest in the variability of this mass flux field was triggered by root cause analyses concerning neutron noise amplitudes, fuel assembly bow and grid-to-grid fretting in classical German PWRs.

For most safety analyses it has been sufficient to assume that the moderator velocity inside the active core region has only a vertical component. On the other hand it had already been inferred from early scaled down flow experiments [1] that the mass flux at the core inlet is higher in the center than at the periphery with a gradient of the order of about 10% and will balance out via cross-flows. In order to better understand the static and dynamic load on the fuel assemblies and to optimize their mechanical design the question if state-of-the-art CFD calculations could confirm the uneven mass flux distribution at core inlet and whether the resulting flow pattern is stationary or to what extent it can be expected to fluctuate in time had been raised. Moreover it has become of interest how sensitive this mass flux pattern is to small changes in thermal-hydraulic boundary conditions, e.g. a change in pump head or a change in downcomer eccentricity.

Historically the standard procedure for testing the mechanical integrity of fuel assemblies under normal operating conditions has been to subject them to flow tests in single assembly or small group assembly flow test rigs. In this manner excitation of resonance oscillations of fuel assemblies could be identified and eliminated. In recent years as demands for reliability have grown the focus of safety analysis has shifted to understand core-wide effects affecting fuel assembly mechanical integrity such as collective fuel assembly bow and zone-wide grid-to-grid damages. While in the late 1990s fuel assembly bow was understood to be caused by differential guide tube growth and was subsequently eliminated by use of irradiation-induced-growth resistant materials, today the issue is static and dynamic fuel assembly bow induced by core wide moderator cross flows.

In order to start developing answers for these questions and to have a good understanding of the physical phenomena, a three-dimensional CFD model was developed for the classical German 1300 MWe PWR reactor type [2]. So far the CFD model has been used to study the pressure drop, flow distribution and mixing in the lower vessel. The vessel has a four-loop primary coolant cycle, 193 fuel assemblies with an active, cold core height of 390 cm and a total of 61 black control rods. The drive mechanism for the control rods and the reactor instrumentation tubes are solely located in the upper pressure vessel region which means that the lower vessel plenum exerts very little flow resistance on the moderator streaming in from the downcomer.

2. LITERATURE REVIEW

The limited capacities of numerical solution methods and computer hardware made it difficult in the past to quantitatively predict the three-dimensional dynamic flow phenomena in the vessels of light water reactors. The situation has been changed recently by the fast development of CFD software and hardware techniques. Table 1 shows a summary of selected publications of CFD analysis concerning the nuclear reactor pressure vessels (RPV) [3-30]. These studies have the essential aim to simulate the 3D flow phenomena in highly complex and huge systems.

The scales of interest are spread over several orders of magnitude in the RPV system. It typically has a height of about 10 m while the thickness of the fuel assemblies' mixing vanes is in the order of 1 mm. To resolve the system in all details would require a CFD mesh far beyond normal computational capabilities. It is found in the literature review that the CFD mesh number has been increased from 10^4~10^5 to 10^8~10^9 during the last fifteen years. Sensitivity studies regarding the computation mesh and the numerical and physical models are made widely in the vessel CFD calculations. The validation of the CFD models need to be carefully performed by comparing the simulation results with available measurements. However

most experimental data available concerns gross quantities like overall pressure loss or static temperature distributions. It is important to notice that to continuously develop CFD models with more advanced methods, better experimental data and instrumentation techniques need to become available from full scale vessel measurements.

Table 1 Selected publications of CFD analysis in RPV

Name	Year	Vessel	Software	Time*	Turbulence**	Mesh type***	Mesh Number	Ref. No.
Gango	1997	PWR	Phoenics	T	T1	M1	$70x10^3$	[3]
Jeong et al.	2006	PWR	Star-CD	S	T1,T3,T4	M2	$5x10^6$	[4]
Cartland Glovere et al.	2007	Test	CFX	T	T2	M1,M2	$4x10^6$	[5]
Rohde et al.	2007	Test	CFX, Fluent	T	T1,T2,T3,T4	M1,M2	$1.3x10^7$	[6]
Fournier et al.	2007	PWR	Code_Saturne	S	T1	M1	$0.5x10^6$	[7]
Bieder et al.	2007	Test	Trio_U	T	T5	M2	$10x10^6$	[8]
Dury et al.	2008	Test	CFX	T	T1,T3	M1,M2, M5	$1.6x10^6$	[9]
Böttcher	2008	PWR	CFX	S	T1	M1,M2	$1.4x10^7$	[10]
Xu et al.	2010	PWR	Star-CCM+	S	T1	M3	$4x10^7$	[11]
Conner et al.	2010	PWR	Star-CCM+	S	T1	M3	$1.9x10^8$	[12]
Pochet et al.	2010	PWR	CFX	S	T1	M2	$5x10^6$	[13]
Karoutas et al.	2010	PWR	Star-CCM+	S	T1	M1,M4	1.2×10^8	[14]
Petrov et al.	2011	PWR	STAR-CD	S	T1	M1,M4		[15]
Chiang et al.	2011	PWR	SC/Tetra	S	T1	M2	$1.2x10^7$	[16]
Kao et al.	2011	PWR	Star-CCM+	S	T1	M3,M4	1.6×10^7	[17]
Jayaraju et al.	2013	Test	Star-CCM+	T	T6	M4	$1.5x10^7$	[18]
Liu et al.	2013	PWR		S	T1	M2	$3x10^6$	[19]
Zhang et al.	2013	PWR	CFX	S	T2	M2	$5.4x10^7$	[20]
Ayhan et al.	2013	PWR	Fluent	S	T1	M2	$1.1x10^7$	[21]
Lee et al.	2014	PWR	CFX	S	T1,T2	M1	$7x10^7$	[22]
Ramajo et al.	2014	PHWR	OpenFOAM	S	T5	M2	$2.6x10^7$	[23]
Toppila et al.	2014	PWR	Fluent	T	T1,T2	M1	$8x10^5$	[24]
Martinez et al.	2014	PWR	Star-CD	S	T1	M1,M2	$1.8x10^8$	[25]
Boyd et al.	2014	BWR	Star-CCM+	S	T1	M4	$2.2x10^7$	[26]
Boumaza et al.	2014	Test	CFX	T	T1	M1,M2	$1.7x10^6$	[27]
Sharabi et al.	2014	PWR	Fluent	T	T1	M1	$5x10^6$	[28]
Cheng et al.	2014	PWR	Star-CCM+	S	T1	M4	$6.5x10^7$	[29]
Mao et al.	2015	PWR	CFX	S	T2	M2	$4.5x10^7$	[30]

*Time: T, Transient; S, Steady-state
** Turbulence: T1, k-ε; T2, k-ω(SST);T3,RNG; T4,RSM (Omega BSL);T5, LES (SGS);T6,LES (WALE)
***Mesh: M1, Hexahedral; M2, Tetrahedral; M3, Trimmed/Cut cell; M4, Polyhedral; M5, Pyramid

Given the necessary limitation about the minimum mesh size, the predictive power of numerical prediction methods depends to a great extent on the performance of the turbulence model used. The

computing capacity is still a limiting factor for CFD turbulence studies in a full scale vessel. RANS (Reynolds-average Navier-Stokes) turbulence models are the most common methods used in the full scale simulation of RPVs. Some other turbulence models (for example: Large eddy simulation, LES) have been reported to be superior to RANS turbulence models in some flow scenarios, however, there is no universal turbulence model that is best for all flow conditions.

Perturbations associated with transients in the flow rate applied by a pump can lead to the fluctuations of flow, temperature and boron concentration at cold leg inlet. Several research groups attempted to apply transient CFD simulations to study the dynamic hydrodynamic phenomena in a PWR vessel. The fluctuations of temperature may cause a feedback to the flow field due to the density variations. The use of CFD to study transient phenomena by coupling flow, temperature and boron concentration fields is still a challenging task even with the most advanced computing resources.

There has been continuous progress in the development of commercial CFD programs, open source codes and in-house codes. Most of the commercial codes are attractive to use because of intuitive use of pre- and post-processing tools. In the nuclear industry, CFD codes for use in large scale vessel calculations still require to be improved with regard to numerical stability, easy to use for the large mesh sizes required, robustness and computational efficiency. Most of the published RPV CFD works have been done by using commercial CFD programs. There are some publications using the open-source codes or in-house developed codes.

3. CFD MODEL DETAILS

3.1. Computational domain and mesh

To create the geometry for the CFD calculation, the first step is to build up a 3D CAD model for a classical German PWR vessel including the reactor internals and the fuel core. The CAD software Creo Parametric (V2.0) was used to construct the PWR vessel. Emphasis in the CAD development has to be placed on future mesh construction and de-featuring in order to avoid mesh mismatching and numerical difficulties in the subsequent CFD analysis. CAD operation to merge, replace, and simplify faces are applied to reduce mesh complexity.

The main objective of the first step development is to study the flow pattern entering the downcomer, flow mixing and redistribution in the lower plenum. The geometrical details in upper plenum are not included. The upper plenum part is considered as an empty part in order to set up the outlet boundary conditions at hot leg outlets. This simplification is considered to have minor effect to flow in the lower plenum. A flow calculation domain is shown in Figure 1. The calculation domain is divided into five parts: cold leg inlet, downcomer, lower plenum, fuel core and hot leg outlet. The fluid domain was created by using Ansys Designmodeler. To simplify the meshing process, the five fluid volume parts have been meshed separately. The meshes of the single parts are connected by contact interfaces, which can be different types depending on the CFD code that will be used to carry out the simulations.

To build an appropriate CFD mesh for highly resolved calculations was one of the most challenging tasks in this study. Different meshing technologies were evaluated. Tetrahedral meshes are generally suitable for complex geometries. Hexahedral meshes have the advantage of high numerical accuracy. However, it is difficult to have a conformal mesh at the contact interfaces. A polyhedral mesh is derived from the tetrahedral mesh by forming polygons around each node in the tetrahedral mesh, which is considered to have advantages in efficiency and accuracy. However, it requires high quality tetrahedral mesh to be converted into polyhedral mesh. A prism boundary layer mesh is needed to use the wall function to resolve the friction near the bounding walls. The prism boundary meshes are difficult to build up when solid structures are complex.

Figure 1 shows the hybrid mesh created by Ansys Meshing (ANSYS R15.0). The multi-zone meshing method was applied and the generated mesh can be used for the Ansys Fluent or CFX solver. Figure 2 shows a high quality trimmed hexahedral mesh created by the CFD code Star-CCM+. The surface mesh was generated first. Then the volume mesh was built based on the surface mesh by adjusting the growth rate and the biggest mesh size. The reference mesh size is 1 cm. Table 2 shows the mesh numbers in different regions. The results of different mesh configurations will be analyzed in the future work. In this paper, the CFD results by using the trimmed mesh (mesh 2) are given in the next sections.

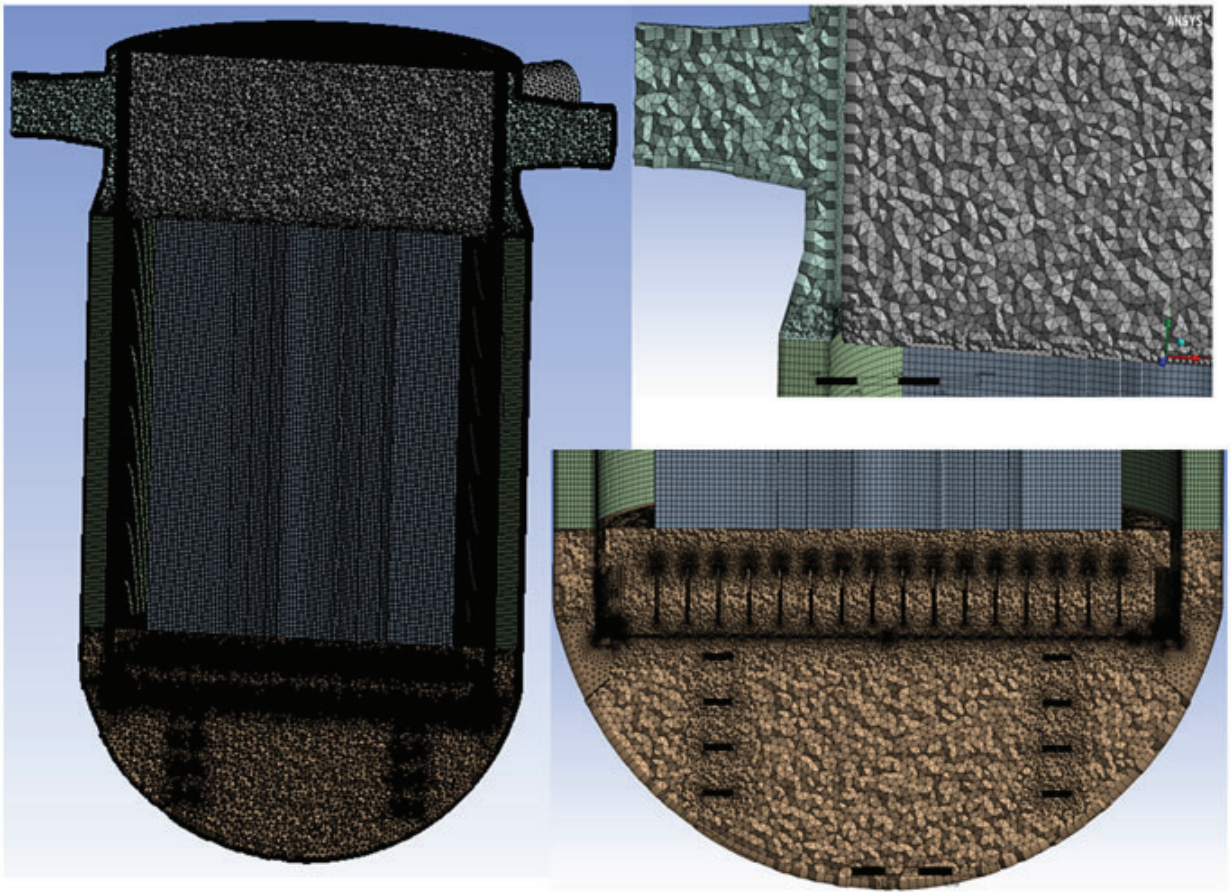

Figure 1 Fluid simulation domain and hybrid meshes (mesh 1)

Table 2 CFD mesh information

Regions	Mesh1 (Hybrid) Volume mesh (x 10^6)	Mesh 2 (Trimmed) Volume mesh (x 10^6)	Mesh 2 (x 10^6) boundary faces	Mesh 2 (x 10^6) internal faces
Cold leg inlet	1	3.8	1.7	11
Downcomer	0.9	8.5	3.5	25
Lower plenum	74	104	22	310
Fuel Core	0.9	3.5	1.7	10
Hot leg outlet	1.2	4.2	2.1	12
Total	78	124	31	368

3.2. Computational details

The calculation of single-phase incompressible flow and mixing is accomplished by solving the mass,

momentum, turbulence and scalar equations. The advection and diffusion terms are treated separately in the mixing process. The local scalar concentration gradients are smoothened out by turbulence and molecular diffusion. The turbulence on mixing is implemented in the diffusion coefficient. The local turbulent diffusion coefficient is calculated with a given turbulent Schmidt number (0.9) from eddy viscosity produced by the turbulence model used.

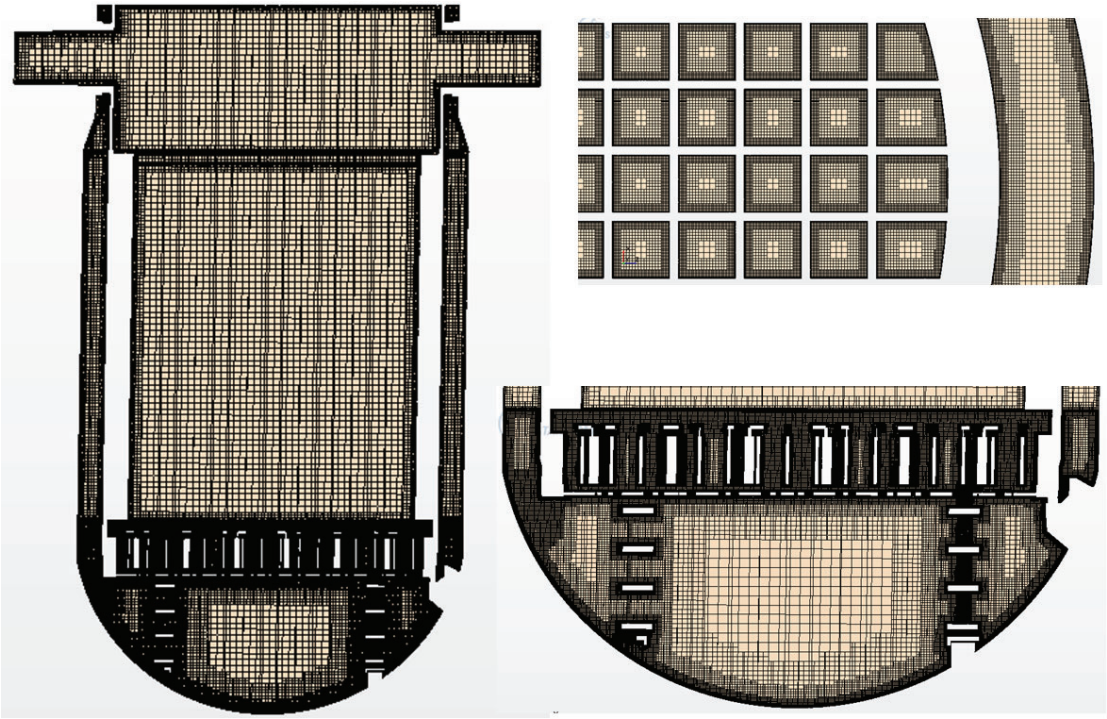

Figure 2 Trimmed hexahedral CFD meshes (mesh 2)

The CFD calculations were done by employing the commercial CFD code -- Star-CCM+ (V9.06). The three-dimensional steady state flow field is solved first. Then in the given solved flow field, a transient mixing is calculated by solving the scalar concentration equation. The second-order upwind scheme is used to calculate the convective flux. The discretized equations were solved in a segregated manner with the semi-implicit method for pressure-linked equations (SIMPLE) algorithm. [31,32] A velocity boundary condition is used at the cold leg inlet nozzle. A wall function (two-layer all y+ wall treatment) is applied to bridge the viscous sub-layer and provide near-wall boundary conditions for the average flow and turbulence transport equations. The wall conditions are connected by means of empirical formulae to the first grid node close to the solid surfaces [33]. The surface average y+ value is 280. The input parameters for simulation are listed in Table 3. Pressure outlet boundary conditions (P_{ref}=0) are used at the hot leg outlets.

Table 3 Process parameters and physical properties

Parameter	Dimension	Value
Inlet velocity	m/s	16.3
Density	kg/m^3	697.3
Viscosity	Pa·s	$8.4 * 10^{-5}$
Pressure	bar	158
Inlet Temperature	^oC	293.8
Inlet scalar concentration	[-]	1
Outlet relative pressure	Pa	0

To reduce computational time and effort the porous media approach for the fuel core region is applied. Porous media are modeled by the addition of a momentum source term to the standard fluid flow equations. The source term is composed of two parts: a viscous term and an inertial loss term. The spacer grids are simplified solid materials and are uniformly dispersed in the flow domain. The porosity and flow resistance replicate the volume-average characteristics of their real geometrical domain. The pressure loss in the fuel core was mainly taken into account in the porous media model based on Westinghouse fuel pressure test results. The under relaxation parameters of flow calculations are pressure (0.1), velocities (0.3) and turbulence (0.5). The calculations on a LINUX cluster with 48 cores (CPU XEON E7-8857 3.0 GHz, 1.5TB RAM) took 180 hours.

4. RESULTS

4.1. Pressure drop

Figure 3 shows the pressure drop along 6 different streamlines (plotted in Figure 4) which were seeded along a line at cold leg nozzle inlet. The center of the cold leg inlet nozzle is defined as zero position in depth. The pressure distribution at the cold leg inlet region has a high variation depending on the positions. Due to the strong momentum driven flow at the inlet nozzle, the inlet jet flows with high horizontal velocity and hits the inner wall of the vessel and thus creates a local high pressure region (red color). The pressure decreases quickly in the circular ring when the fluid changes the flow direction downwards. About 1.5m downward along the z-axis (the upper part of the downcomer) the pressure is unevenly distributed with a variation of about 0.6 bar.

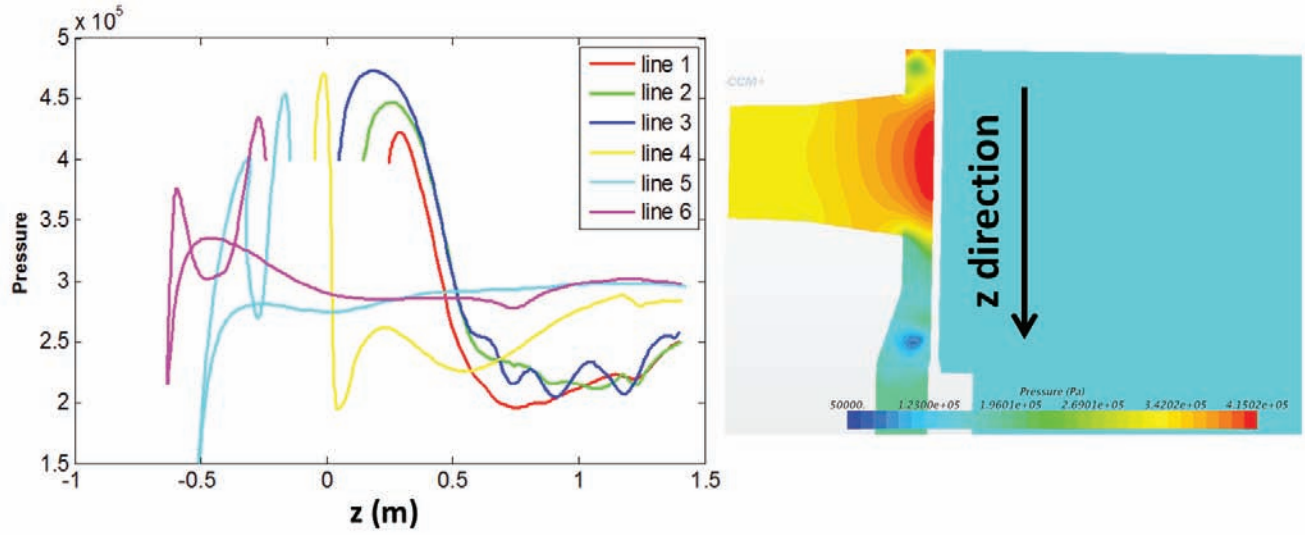

Figure 3 Pressure drop along 6 streamlines in cold leg inlet region

Figure 4 shows the pressure drop along the same streamlines as in the figure 3 in the lower plenum region. The starting positions are in the downcomer and the ending positions are in the upper part of the lower plenum (both of them are at the 6.2 m level below the cold leg inlet nozzle). Two main pressure drop regions can be observed. One is the flow expansion pressure drop of about 0.2 bar when the fluid stream leaves from the circular downcomer entering the reactor bottom. Another is the fluid flow through the multi-hole orifice plate, which causes a big pressure drop of about 0.7 bar. While flowing through the multi-hole orifice plate, the fluid undergoes a flow contraction that is followed by a flow expansion. During flow contraction the flow velocity increases and the static pressure decreases. During the flow expansion after passing through the holes, the flow velocity decreases and the static pressure increases. A pressure recovery is observed in Figure 4 of about 0.2 bar.

The calculated surface average pressure drops through vessel are listed in Table 4. The calculated pressure drops are in reasonable agreement with plant engineering data. In this work, no bypass flow was modeled and thus 100% of the coolant flows through fuel region, which leads to a slightly higher pressure drop. The pressure drop in upper plenum is not listed in the table due to the detailed flow structure in the upper plenum which is not included in this CFD model.

Table 4 Calculated pressure drop by using surface average values

Cold leg inlet	DP(downcomer)	DP (Lower plenum)	DP (Fuel Core)
0.99 bar	~0.01 bar	0.5 bar	1.15 bar

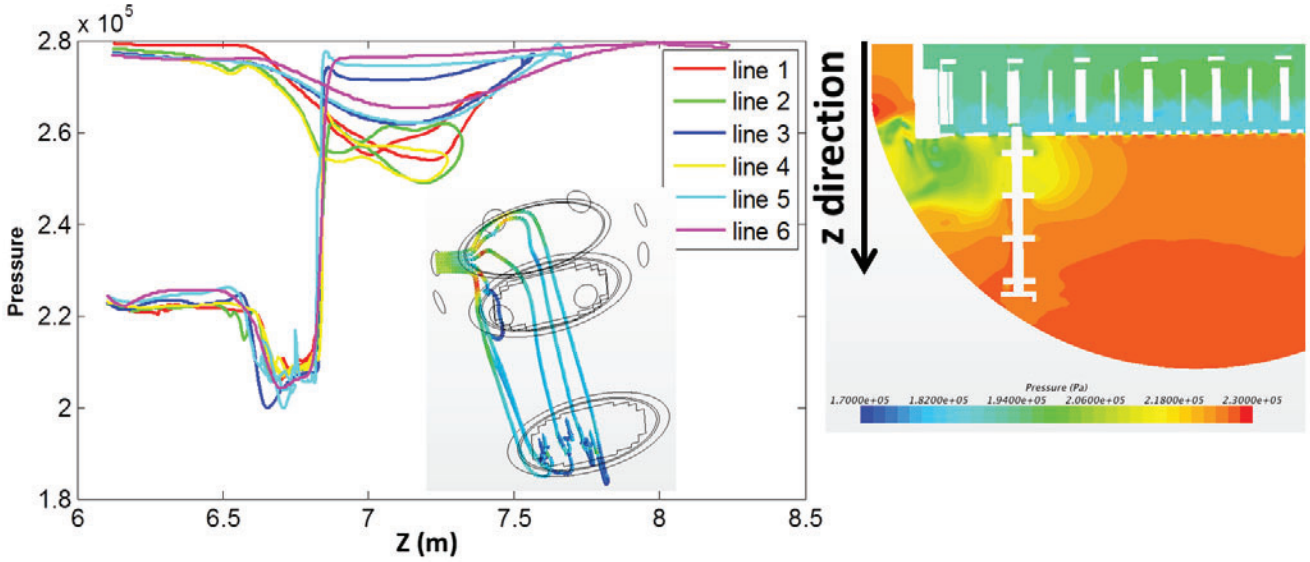

Figure 4 Pressure drop along 6 streamlines in lower plenum region

4.2. Flow distribution

Two cases with four and three loop operation have been calculated in order to compare two limiting cases of flow patterns. Loop 4 is the non-operating loop in the three loop case. Figure 5 displays the velocity magnitude at cutting planes z=0m (center of cold leg inlet nozzle) and z=5.6m (close to fuel core inlet). The calculation shows maximum velocities exist at azimuthal positions between two inlet and two outlet nozzles in the lower part of the downcomer (Figure 5c). The flow distribution in the downcomer shows a good qualitative agreement with published results of both LDA measurements and CFD calculations [6]. The locations of minimum flow velocities are directly below the inlet nozzles. In the 3 loop case (Figure 5d) a maximum velocity region is located between the two inlets on the right side opposite to where the blocked loop lies. The lowest velocity region is below the cold leg inlet on the left hand side. Due to the strong momentum driven flow at the inlet nozzles, the horizontal velocities are high in the upper part of the circular ring. The inlet flow from the unpaired cold leg nozzle is distributed into two main jets after entering the downcomer. It looks like a butterfly distribution. This is the main reason why the center of the flow distribution is shifted towards the non-operating loop side and the velocity is higher below loop 4 compared with operating loop 3.

Figure 6 gives the flow distribution at fuel core inlet for the 4 loop and 3 loop cases. A noticeable inlet velocity distribution was found in the center of the core. This can be confirmed by early scaled down test results and the velocity variation at the core inlet is in the order about ± 10%. In the 3 loop case test results from the same scaled down experiments show a somewhat higher velocity variation in the order of about ±14%. CFD calculated results confirm the magnitude of the increased velocity variation.

The center of the mass flow region at the core inlet is shifted to the left side towards the non-operating loop 4 in the 3 loop case. In order to understand this phenomenon in more detail Figure 7 shows the velocity comparison at a slice cutting plane in the lower plenum (cutting positions marked by dotted line in Figure 6). A symmetrical flow pattern is observed in the 4 loop case. In the 3 loop case the fluid at the right side entering the lower plenum from the circular ring has a higher momentum and this high velocity stream flows deeper downward along the right side wall to towards the center of the lower part of the plenum. Thereby, the flow stagnation region (dark blue color in the bottom of vessel) is shifted to the left side and is also mirrored in the above mentioned butterfly like flow redistribution from the unpaired loop Since the static pressure is higher in the stagnation region the flow pattern has a higher mass flow at the left side of the core inlet as shown in Figure 6b compared to the 4 loops case in Figure 6a.

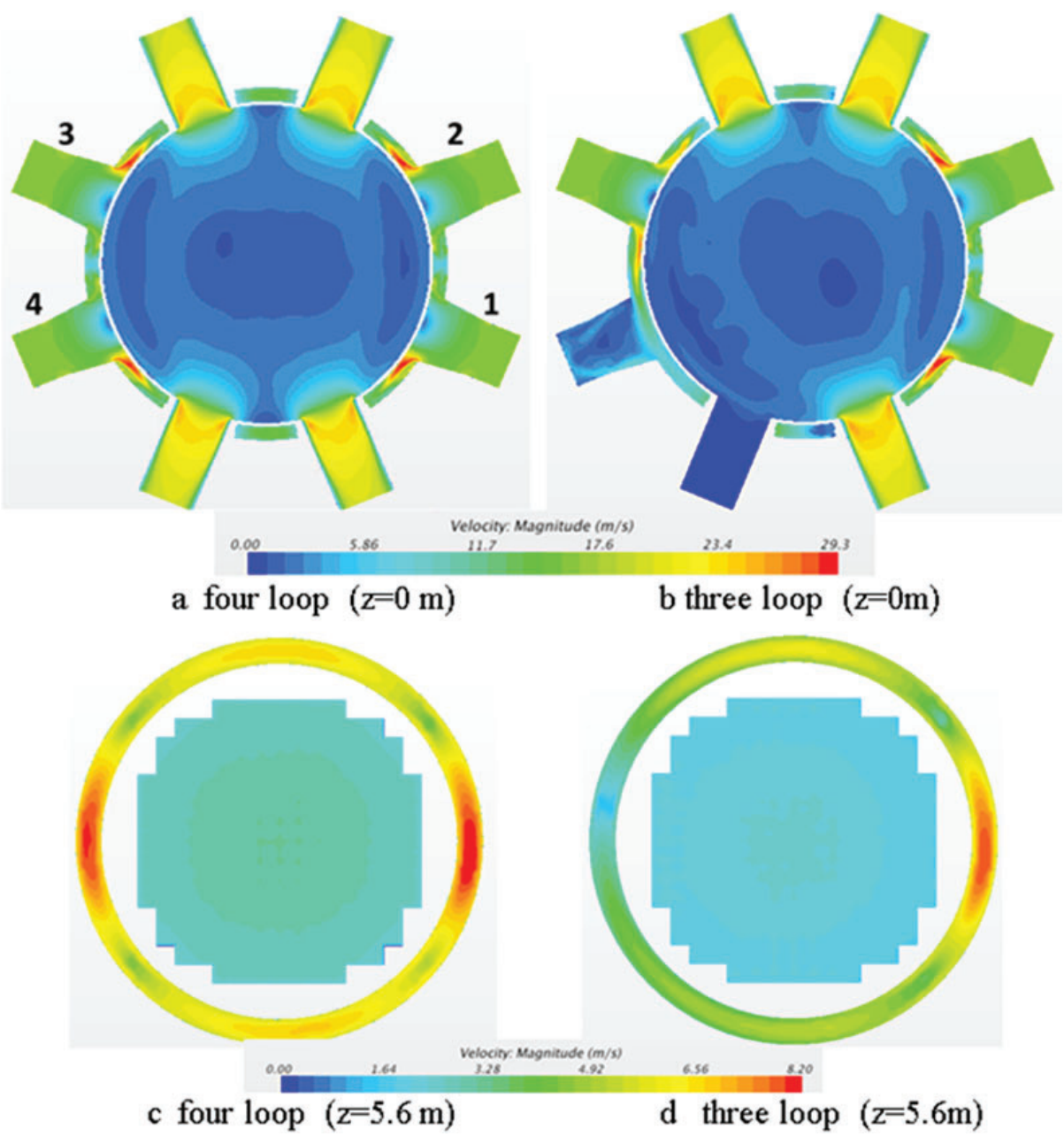

Figure 5 Streamlines and velocity at cutting planes (z=0, 5.6m) for four and three loop operation

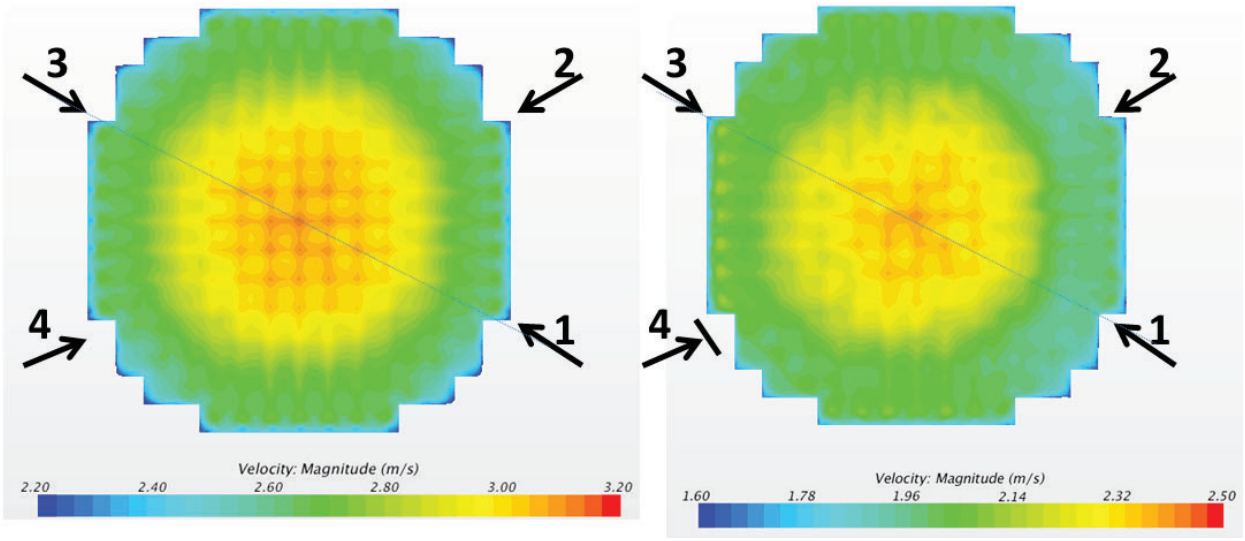

a) 4 loop **b) 3 loop**

Figure 6 Flow distributions at the fuel core inlet for two different cases

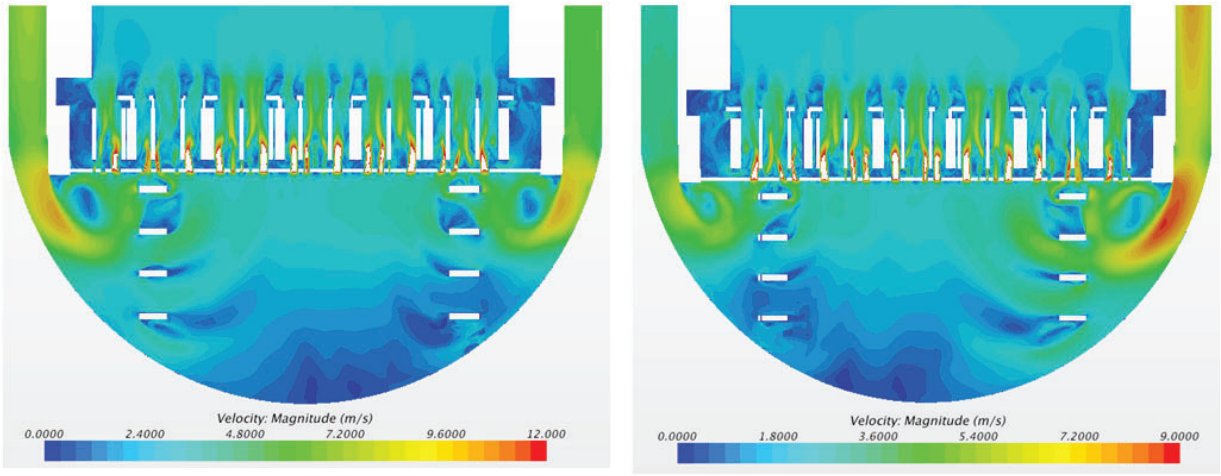

a) 4 loop **b) 3 loop**

Figure 7 Flow distributions in lower plenum for two different cases

4.3. Mixing

A steady state mixing study has been carried out for 4 loop and 3 loop operations to further investigate the character of the fluid flow field through the core. A passive scalar equation was solved to calculate the dimensionless concentration distribution. The inlet boundary condition of the passive scalar is set to one at the cold leg inlet 3. At the other cold leg inlets, the scalar is set to zero. Figure 8 shows the concentration distribution at two slice planes (z=0, 5.6m). The highest concentrations are located in one quarter of the vessel below cold leg 3 and hot leg 3.

For the 4 loop case the interactions between the loops are weak. This means that water entering a specific loop also exists again into that loop after the core passage. In the 3 loops case the interactions between loop 3 and 1 is becoming stronger. The high concentration stream from inlet 3 tends to flow to both hot leg 3 and with reduced intensity into hot leg 1.

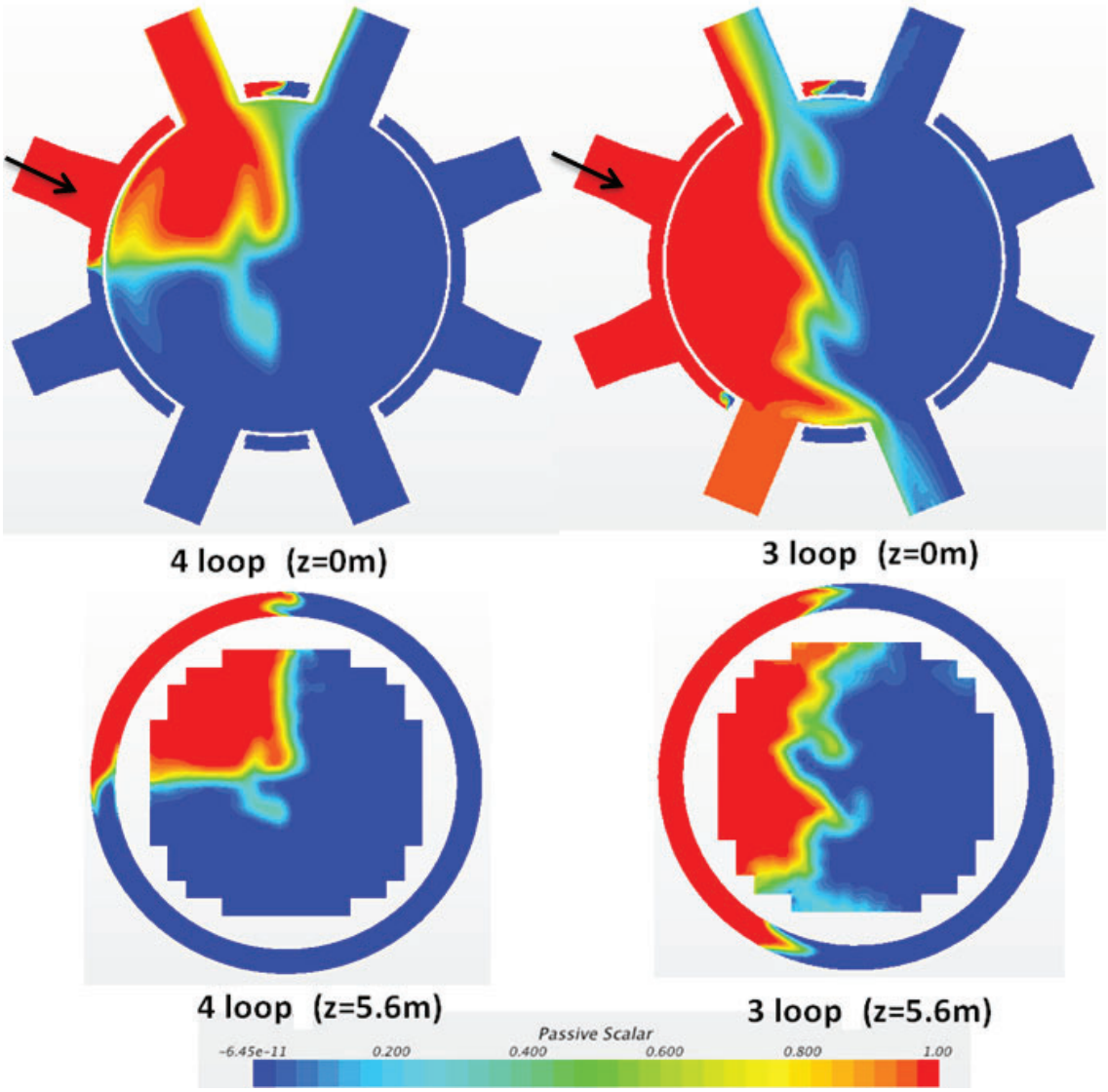

. **Figure 8 Concentration distributions for 4 loop and 3 loop cases**

A 15 seconds transient mixing simulation for the 3 loop operation has been performed. In the first step of this study, the steady state flow field has been calculated first, then the flow field is frozen and finally the transient passive scalar equation is solved. Time step size was 0.1 s. It is assumed that there is continuous concentration injection at cold leg inlet 3. The starting time for injection is time zero. Figure 9 shows the calculated transient concentration distributions at core inlet at 2, 3 and 4 seconds. Two separate high concentration regions are observed, which indicate the flow is separated into two streams in the downcomer according to the butterfly pattern mentioned earlier. This phenomenon was also observed in an earlier experiment [6]. After four seconds, a quasi-steady state concentration distribution is observed. From the transient and steady concentration distribution (Figures 8 and 9), it is found that the most flow mixing and redistribution has happed in the downcomer and lower plenum. However, it should be pointed

out that a porous media model is applied in the core region in this CFD model. In order to accurately predict the flow redistribution in the core region, the further development of CFD model to include the geometrical details of fuel core is necessary. To save the CPU times, the steady state flow pattern is used for the mixing studies in the first step of study. In the next step, the transient flow and mixing simulations will be performed.

The average concentration at the core inlet and outlet plane is shown in the right side of Figure 9. Figure 9 shows that the residence time for the mixing concentration in the fuel core region is about 2 seconds by comparing the core inlet and outlet concentrations. In this calculation a porous media model was applied in the fuel core region. In the real case, the flow area in the fuel core region is smaller due to the solid parts such as fuel rods and space grids. The channel flow velocity is thus higher compared with porous media model results. Therefore, the real residence time of mixing concentration becomes shorter. After 10~12 seconds from starting time, the average concentration at fuel inlet and outlet reach a constant value 0.33, which is a reasonable result for 3 loop operation case.

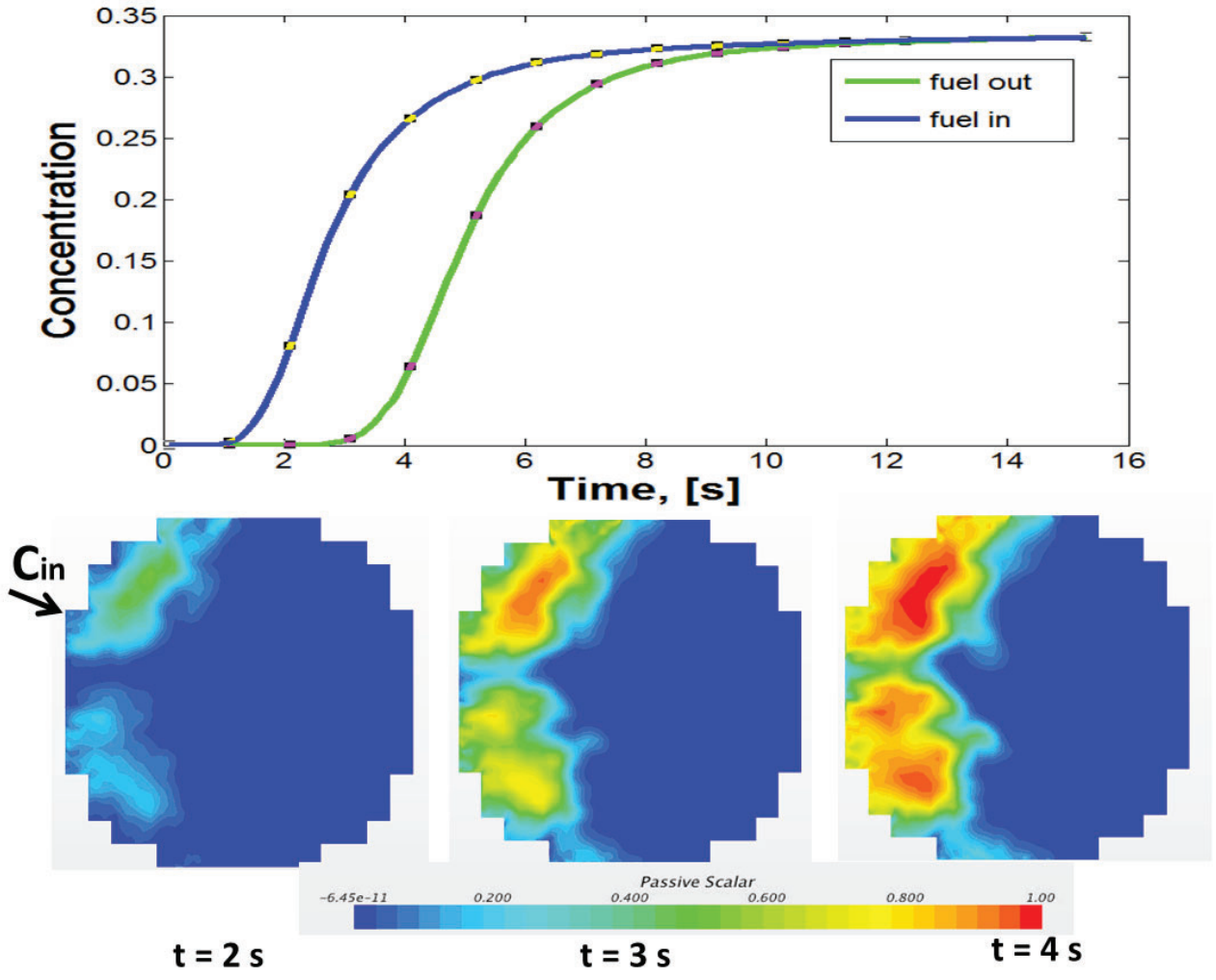

Figure 9 Transient surface average concentration at core inlet/outlet and concentration contour at core inlet

5. DISCUSSION AND FUTURE WORK

The aim of this study is to develop a full scale PWR vessel CFD model to investigate the dynamic hydraulic phenomena. The preliminary results show the potential of the CFD model to improve the understanding of the flow mixing behavior in the vessel and aid the engineering design.

In the Nuclear Energy Agency (NEA) best practice guidelines for the use of CFD [34], it is noted that geometrical details of vessel internals have a strong influence on the flow field and hence on mixing. Hence, the geometrical details in the lower plenum are included in the current CFD model. However, it is not an easy task to decide which details are relevant. One challenging problem is the numerical burden by the massive mesh needed for the calculations. Table 2 shows that the lower plenum requires a large mesh in order to achieve sufficient accuracy. In case of a model of the entire core including details of the fuel rods and space grids, it has been estimated that a mesh of about three billion cells would be required. To build up such a big CFD model, a number of technology gaps and impediments need to be overcome. Specially, they are:

1. The Access to a supercomputer machine with High Performance Computing technology (HPC). The big CFD model is clearly beyond the current hardware and software capabilities of a normal industrial company. In order to capture the dynamic flow behavior in the vessel transient simulations need to be performed. It is estimated that 5 million CPU hours are required to simulate a 5 minutes transient case with time step size 1 ms. The cost per CPU hour in available supercomputer centers with a normal service rate is not economical for this case which will require many necessary iterations to build up a reliable calculation. Therefore, it is important to either share costs between industries, supercomputer centers at universities and research institutes or to develop distributed computing methods on comparatively cheap hardware solutions.

2. To develop signatures and methods for numerical stability for a complex system. In contrast to the rapid development of high-order numerical algorithms in CFD, the applications of high-order and high accurate numerical methods on complex configurations are still limited. One of the reasons is mainly derived from the complexity of the CFD mesh. We have divided the vessel into several parts to mesh them separately. The convergence is sensitive to the mesh configurations between contact interfaces for different parts. Although many CFD codes are able to demonstrate convergence for a few simple problems, for flow simulations with very complex geometry many of current solver techniques employed may fail or require significant user intervention to obtain reliable results.

3. To improve the required methods of large data management. For one case of a full scale transient PWR CFD simulation including all geometrical details, the CFD-generated data file size could be over 1000 TB. Methods for massive data transfer, storage and data extraction from large datasets need to be developed. Methods to process and visualize large scale transient simulations in real time are required to support the advance CFD applications.

In summary the following two steps need to be easily iterated in building a reliable, dynamic CFD calculation for a RPV. Step 1: CAD, CFD geometry preparation and mesh generation. It is important to build a high quality mesh which helps the CFD solver converge to the reliable answer while minimizing the computer resources expended. Step 2: CFD model set-up, calculation, post-processing and analysis of numerical uncertainty. The tools for CAD and CFD mesh manipulation in our view need much more improvements to facilitate the many Step 1 and Step 2 iterations necessary for our purposes. Tools need to incorporate dedicated scripting capabilities to help handle and manipulate the large information containers.

As the confidence in the CFD model growth it will be stepwise scaled up. The geometrical details will thereby be gradually increased in the model. The porous medium approach for the fuel core was used in the beginning. The porous region will be gradually replaced by a real geometry following with the CFD model scale-up. A middle-scale CFD model is expected to be built up with the mesh number around 100~500 million. The transient time scale is up to 30 seconds. These calculations can be performed in an industry CFD cluster. It is an important intermediate stage for the development. A sensitivity study on different numerical aspects of the CFD model, including mesh size, numerical algorithms, and time step size etc. will be carried out. A sensitivity study on different physical model set-ups, including turbulence model, porous media model will be investigated. An important task is to validate the developed CFD model by comparing with the experimental results, plant measurements or previous published results.

Finally a long-range research plan is necessary for developing a large scale PWR vessel CFD model including the considerations of 1) ability to effectively utilize massive HPC architectures; 2) reliable numerical methods in software; 3) high degree automation in analysis process; 4) collaboration between industry, university and research institute; 5) explicit collaboration with other community, such as turbulence research, weather prediction and computational aeroscience.

6. **CONCLUSION**

A three-dimensional CFD model was developed to study the pressure drop, flow distribution and mixing in a classical German PWR reactor. The calculation domain has been made up of 5 parts: cold legs, downcomer, lower plenum, fuel core and hot legs. In order to understand the core inlet flow distribution the geometrical details in the lower plenum have been included in the model. A porous media model is used in the fuel-core region as a simplification for this stage of the work. A full scale 3D CAD model was used to create the fluid domain for the generation of CFD meshes.

For verification purposes of the CFD model the pressure drops along the cold leg inlet, the downcomer and the lower plenum were compared with plant engineering data and showed good agreement. Moreover the flow and concentration behavior for 3 and 4 loop operations have been calculated and compared to results from existing scaled down experiments. Results show that steady state flow fields and quasi-static mixing calculations are reliable. Future plan is to utilize the vessel CFD model for the thermal hydraulic analysis, such as lower plenum flow anomalies, boron dilution, thermal mixing and core flow distribution.

To develop a large scale CFD model, the technology gaps and impediments are discussed, including 1) the assessment to supercomputer machine with High Performance Computing technology; 2) the development of numerical stability for a complex system; 3) the method improvements of large data management. The next steps in our multi-staged developing plan have been outlined.

In summary this research targets to answer a number of practical questions facing utilities with regard to fuel assembly design and the boundary conditions for in-core safety analysis: i.e. the magnitude and frequency behavior of core-wide radial forces acting on fuel assemblies and to which extent they could lead to collective fuel assembly bow and to zone-wide grid-to-grid fretting. Furthermore the sensitivity of the underlying core-wide cross flows with regard to external perturbations stemming from the coolant pumps or from down-comer eccentricity is addressed. The last point is important because it answers the question whether improvements in fuel assembly mechanical stiffness or improvements in mechanical stability of ex-core components are better suited to reduce grid-to-grid fretting or collective fuel assembly bow. Finally the prediction of the core-inlet mass flow distribution is relevant to the margin calculation of fuel assembly hold-down springs in 4-loop and 3-loop operation and during the transition from 4- to 3-loop operations and vice versa. In a later stage this research can be combined with measured temperature profiles from reactor cold legs to address questions regarding the magnitude and frequency distribution of core-inlet temperature fluctuations to predict the magnitude of reactivity induced neutron noise.

REFERENCES

1. G. Ulrych and E. Weber, "Neuere Ergebnisse zur Kühlmittelströmung in Druckwasserreaktoren", *Atomkernenergie-Kerntechnik,* **42**(4), pp. 217-223 (1983)
2. J. Czech, A. Feigel and P. J. Meyer, "Technical information on design features of Siemens Konvoi PWR", *IAEA-TECDOC-861*, pp. 145-170(1994)
3. P. Gango, "Numerical boron mixing studies for Loviisa nuclear power plant", *Nuclear Engineering and Design*, **177**, pp. 239-254 (1997)
4. J. H. Jeong, J. P. Park and B. S. Han, "Head loss coefficient based on CFD analysis for PWR downcomer and lower plenum", *Transactions of the Korean Nuclear Society Autumn Meeting*, Gyeongju, Korea, November (2006)
5. G. M. Cartland Glover, T. Höhne, S. Klien, U. Rohde, F. P. Weiss and H. M. Prasser, "Hydrodynamic phenomena in the downcomer during flow rate transients in the primary circuit of a PWR", *Nuclear Engineering and Design*, **237**, pp. 732-748 (2007)
6. U. Rohde, T. Höhne, S. Kliem, B. Hemström, M. Scheuerer, T. Toppila, A. Aszodi, I. Boros, I. Farkas, P. Muhlbauer, L. Vyskocil J. Klepac, J. Remis and T. Dury, "Fluid mixing and flow distribution in a primary circuit of a nuclear pressurized water reactor-Validation of CFD codes", *Nuclear Engineering and Design*, **237**, pp 1639-1655 (2007)
7. Y.Fournier, C. Vurpillot and C. Bechaud, "Evaluation of fluid flow in the lower core of a PWR with *Code Saturne", Nuclear Engineering and Design*, **237**, pp. 1729-1744(2007)
8. U. Bieder, G. Fauchet, S. Betin, N. Kolev and D. Popov, "Simulation of mixing effects in a VVER-1000 reactor", Nuclear Engineering and Design, *Nuclear Engineering and Design*, **237**, pp. 1718-1728(2007)
9. T. V. Dury, B. hemström and S. V. Shepel, "CFD simulation of the vattenfall 1/5th-scale PWR model for boron dilution studies", *Nuclear Engineering and Design*, **238**, pp. 577-589(2008)
10. M. Böttcher, "Detailed CFX-5 study of the coolant mixing within the reactor pressure vessel of a VVER-1000 reactor during a non-symmetrical heat-up test", *Nuclear Engineering and Design*, **238**, pp. 445-452(2008)
11. Y. Xu, K. Yuan, M. B. Dzodzo, M. E. Conner, S. A. Beltz, S. Ray, T. A. Bissett, C. C. Chieng, M. T. Kao and C. Y. Wu, "Computational fluid dynamics analysis of AP1000 reactor vessel upper plenum and top core slab", *Proceedings of 2010 LWR fuel performance/TOPFuel/WRFRM*, Florida, USA, paper 039 (2010)
12. M. E. Conner, Z. Karoutas, S. A. Beltz,, Y. Xu, K. Yuan, M. B. Dzodzo, T. A. Bissett, C. C. Chieng, M. T. Kao and C. Y. Wu, "Study of impact of the AP1000 upper internal design on fuel performance", *Proceedings of 2010 LWR fuel performance/TOPFuel/WRFRM*, Florida, USA, paper 038 (2010)
13. G. Pochet, M. Haedens, C. R. Schneidesch and D. Leonard, "CFD simulations of the low mixing in the lower plenum of PWR's", *Proceedings of the CFD for Nuclear Reactor Safety Applications (CFDNRS-3),* Maryland, USA, 14-16 September (2010)
14. Z. Karoutas, K. Lang and P. Joffre, "Evaluating PWR fuel performance using vessel CFD analysis", *Proceedings of 2010 LWR fuel performance/TOPFuel/WRFRM*, Florida, USA, paper 017 (2010)
15. V. Petrov and A. Manera, "Effect of pump-induced cold-leg swirls on the flow field in the RPV of the EPR: CFD investigations and comparison with experimental results", *Nuclear Engineering and Design*, **241**, pp. 1478-1485(2011)
16. J. Chiang, B. S. Pei and F. P. Tsai, "Pressurized water reactor (PWR) hot-leg streaming Part 1: Computational fluid dynamics (CFD) simulations", *Nuclear Engineering and Design*, **241**, pp. 1768-1775(2011)
17. M. T. Kao, C. C. Chieng, C. Y. Wu, Y. Xu, K. Yuan, M. B. Dzodzo, M. E. Conner, S. A. Beltz, S. Ray, and T. A. Bissett, "CFD analysis of PWR core top and reactor vessel upper plenum internal subdomain models", *Nuclear Engineering and Design*, **241**, pp. 4181-4193(2011)

18. S. T. Jayaraju, P. Sathiah, E. M. J. Komen and E. Baglietto, "Large eddy simulation for an inherent boron dilution transient", *Nuclear Engineering and Design*, **262**, pp. 494-498(2013)
19. J. Q. Liu, B. M. Sun, Z.S. Li, D. L. Zhang, L. Y. Zhou and T. Bai, "Three dimensional numerical simulation on Nuclear reactor interior flow and temperature field of a 1000MW unit*", Research journal of applied science, engineering and Technology* 6(11), pp.2019-2026(2013)
20. M. Q. Zhang, X. B. Ran, Y.W.Liu, X. L. Yu and M.L. Zhu, "CFD simulation analysis and validation for CPR 1000 pressurized water reactor", *Nuclear Techniques*, **36**(10), 100601(2013) in Chinese
21. H. Ayhan and S. Ergun, "Modeling VVER-1200 Reactor pressure vessel by using computational fluid dynamic tools", Proceedings *of BgNS conference, 18*-21 September 2013, Sunny beach, Bulgaria (2013)
22. G. H. Lee, C. Y. Song, Y. S. Bang, S. W. Woo, D. H. Kim and M. G. Kang, "CFD simulation of reactor internal flow in the scaled APR+", *Journal of Energy and Power Engineering*, 7, pp. 1533-1538(2013)
23. D. Ramajo, S. Corzo, N. Schiliuk, A. Lazarte and N. Nigro, "CFD modeling of the moderator tank of a PHWR nuclear Power plant", *Mecanica Computacional*, Vol **XXXIII**, pp 2913-2926 (2014)
24. T. Toppila, J. Kuopanportti and T. Räma, "Assessment of CFD model for Loviisa NPP coolant mixing studies using data of steam safety valve tests", *CFD4NRS-5*, ETH, Zurich, Switzerland, September 9-11(2014)
25. J. Martinez and J. Galpin, "CFD modeling of the EPR primary circuit", *Nuclear Engineering and Design*, **278**, pp 529-541(2014)
26. C. Boyd and R. Skarda, "CFD predictions of standby liquid control system mixing in lower plenum of a BWR", *Nuclear Engineering and Design*, **279**, pp. 109-115(2014)
27. M. Boumaza, F. Moretti and R. Dizene, "Numerical simulation of flow and mixing in ROCOM facility using uniform and non-uniform inlet flow velocity profiles", *Nuclear Engineering and Design*, **280**, pp. 362-371(2014)
28. M. Sharabi, B. Niceno, V.N. Gonzalez-Albuixech and M. Nifferegger, "Computational fluid dynamics study of pressurized thermal shock phenomena in the reactor pressure vessel", *CFD4NRS-5*, ETH, Zurich, Switzerland, September 9-11(2014)
29. W. C. Cheng, Y.M. Ferng, S.R. Chen and C.C. Chieng, "Development of CFD methodology for investigatingthermal-hydraulic characteristics in a PWR dome", *Nuclear Engineering and Design*, **284**, pp. 284-292(2015)
30. H. Mao, C. Ku, H. L. Zhang and P. F. He, "Analysis research on mixing characteristics of lower plenum of Qinshan phase II NPP by CFD method", *Atomic Energy Science and Technology*, **49**(1), pp 47-50(2015) in Chinese
31. STAR-CCM+ 9.06 User's Guide, www.cd-adapco.com
32. S. V. Patankar and D. B. Spalding, "A calculation procedure for heat, mass and momentum in three-dimensional parabolic flows", *International Journal of Heat and Mass Transfer*, pp.15 (1972)
33. B. E. Launder and D. B. Spalding, "The numerical computation of turbulent flows", *Computatioinal Methods in Applied Mechanics and Engineering,* **3**(3), pp. 269-289 (1974)
34. J. Mahaffy et al., "Best practice guidelines for the user of CFD in nuclear reactor safety applications", *NEA/CSNI/R(2007)5*, Paris, France (2007)